

This is the peer-reviewed version of the following article:

Karel Královec, Radim Havelek, Darja Koutová, Pavel Veverka, Lenka Kubičková, Petr Brázda, Jaroslav Kohout, Vít Herynek, Magda Vosmanská, Ondřej Kaman. Magnetic nanoparticles of Ga-substituted ϵ -Fe₂O₃ for biomedical applications: Magnetic properties, transverse relaxivity, and effects of silica-coated particles on cytoskeletal networks. *Journal of Biomedical Materials Research - Part A*. 16 March 2020.

which has been published in final form at <https://doi.org/10.1002/jbm.a.36926>.

This article may be used for non-commercial purposes in accordance with Wiley-VCH Terms and Conditions for Self-Archiving.

This postprint (accepted) version is available from <https://hdl.handle.net/10195/77329>.

Magnetic nanoparticles of Ga-substituted ε -Fe₂O₃ for biomedical applications: magnetic properties, transverse relaxivity and effects of silica-coated particles on cytoskeletal networks

Karel Královec*¹, Radim Havelek², Darja Koutová², Pavel Veverka³, Lenka Kubíčková^{3,4}, Petr Brázda³, Jaroslav Kohout⁴, Vít Herynek⁵, Magda Vosmanská⁶, and Ondřej Kaman*³

¹Faculty of Chemical Technology, University of Pardubice, Studentská 573, 532 10 Pardubice, Czech Republic

²Faculty of Medicine in Hradec Králové, Charles University, Šimkova 870, 500 03 Hradec Králové, Czech Republic

³Institute of Physics, Czech Academy of Sciences, Cukrovarnická 10/112, 162 00 Praha 6, Czech Republic

⁴Faculty of Mathematics and Physics, Charles University, V Holešovičkách 2, 180 00 Praha 8, Czech Republic

⁵First Faculty of Medicine, Charles University, Kateřinská 32, 121 08 Prague, Czech Republic

⁶Faculty of Chemical Engineering, University of Chemistry and Technology, Prague, Technická 5, 166 28 Praha 6, Czech Republic

*Corresponding authors:

This article has been accepted for publication and undergone full peer review but has not been through the copyediting, typesetting, pagination and proofreading process which may lead to differences between this version and the Version of Record. Please cite this article as doi: 10.1002/jbm.a.36926

Karel Královec

Department of Biological and Biochemical Sciences

Faculty of Chemical Technology

University of Pardubice

Studentská 573

532 10 Pardubice

Czech Republic

Tel.: +420466037755

E-mail address: karel.kralovec@upce.cz

Ondřej Kaman

Department of Magnetism and Superconductors

Institute of Physics of the Czech Academy of Sciences

Cukrovarnická 10/112

162 00 Prague 6

Czech Republic

Tel.: + 420220318418

E-mail address: kamano@seznam.cz

Abstract

Magnetic nanoparticles of $\epsilon\text{-Fe}_{1.76}\text{Ga}_{0.24}\text{O}_3$ with the volume-weighted mean size of 17 nm were prepared by thermal treatment of a mesoporous silica template impregnated with metal nitrates and were coated with silica shell of four different thicknesses in the range 6–24 nm. The bare particles exhibited higher magnetization than the undoped compound, $22.4 \text{ A m}^2 \text{ kg}^{-1}$ at 300 K, and were characterized by blocked state with the coercivity of 1.2 T at 300 K, being thus the very opposite of superparamagnetic iron oxides. The relaxometric study of the silica-coated samples at 0.47 T revealed promising properties for MRI, specifically, transverse relaxivity of $89\text{--}168 \text{ s}^{-1} \text{ mmol(f.u.)}^{-1} \text{ L}$ depending on the shell thickness was observed. We investigated the effects of the silica-coated nanoparticles on human A549 and MCF-7 cells. Cell viability, proliferation, cell cycle distribution, and the arrangement of actin cytoskeleton were assessed, as well as formation and maturation of focal adhesions. Our study revealed that high concentrations of silica-coated particles with larger shell thicknesses of 16–24 nm interfere with the actin cytoskeletal networks, inducing thus morphological changes. Consequently, the focal adhesion areas were significantly decreased, resulting in impaired cell adhesion.

Keywords

Epsilon polymorph, Ga-doped iron(III) oxide, transverse relaxivity, cytotoxicity, cytoskeleton

1 INTRODUCTION

Intriguing concepts employing nanostructures, from simple single-phase particles to complex nanoarchitectures such as smart particles with stimuli-responsive coatings and biologically active cargo, nanomatryoshkas with multilayered plasmonic structures or precisely tailored inorganic nanoparticles with multimodal organic functionalization, have been suggested and experimentally demonstrated for advanced medical and biological applications, but those based on magnetic nanoparticles have attracted overwhelming attention and have provided agents already used in clinical practice or subjected to clinical trials. The well-known medical applications, both the present-day as well as prospected options, with magnetic particles as the crucial component include contrast agents for magnetic resonance imaging (MRI), heating mediators for magnetic fluid hyperthermia, carriers for magnetically guided drug delivery and triggered release of drugs by external stimuli, labelling agents for magnetic particle imaging, and a core material for number of diagnostic methods with magnetically assisted separation. However, the MRI, a non-invasive, non-ionising imaging technique of immense importance in medicine and biomedical research, represents an excellent example where magnetic particles of maghemite, magnetite, and mixtures thereof have been routinely used for both diagnostic imaging and tracking of labelled cells [1, 2] while many other types of magnetic nanoparticles based on diverse ferrites, zero-valent iron, certain alloys,[3] or even perovskite manganites [4] have been proposed.

The present study suggests employing nanoparticles of a suitably doped ϵ -Fe₂O₃ phase as a novel and promising magnetic material for medical applications. This choice, unprecedented in literature on nanomedicine, is motivated by the recent report on ϵ -Fe₂O₃ nanoparticles and their silica-coated products, that demonstrated reasonable transverse relaxivity and good performance in MRI,[5] but whose properties could be - in principle - further enhanced by doping, namely by diamagnetic cations with preference for tetrahedral coordination as is rationalized below. The main distinction of the ϵ -Fe₂O₃ nanoparticles compared to the common superparamagnetic maghemite or magnetite particles consists in their magnetically blocked state, i.e. non-superparamagnetic behaviour with high remanence and huge coercivity of 2 T at 300 K [6] given by their large magnetocrystalline anisotropy. Such magnet-like particles offer an interesting and understudied platform for possibly new applications, where the Néel relaxation of magnetic moments of particles in the superparamagnetic state does not occur. Moreover, their large magnetic anisotropy strongly favours the rotational relaxation (Brownian rotation) in AC magnetic fields, which could be useful for the applications of magnetic nanostructures in local mechanical disruption activated by AC fields.

The epsilon polymorph is one of the five structurally different crystalline phases of Fe₂O₃ that are stable under ambient conditions and that exhibit very different magnetic properties [7]. Specifically, the thermodynamically stable and the most abundant form in nature, i.e. the trigonal α -Fe₂O₃ (hematite) is characterized by canted antiferromagnetic order at room temperature, the rare cubic β -Fe₂O₃ phase with the bixbyite structure is paramagnetic above the Néel temperature of 110–120 K, the cubic γ -Fe₂O₃ (maghemite) with the spinel structure and ferrimagnetic ordering from low temperatures up to the limit of its thermal stability is

Accepted Article

routinely employed in MRI, the orthorhombic ϵ -Fe₂O₃ is a collinear ferrimagnetic system between ≈ 160 K and the Curie temperature of 490–500 K, whereas the last one, the monoclinic ζ -Fe₂O₃, albeit stable under ambient conditions, has been achieved only at high pressures of 30 GPa and is paramagnetic above the Néel temperature of 69 K [8]. Among them, the most intriguing is the ϵ -Fe₂O₃ phase with four crystallographically distinct Fe positions, three of which show octahedral coordination while one is characterized by tetrahedral coordination. In the ferrimagnetic state of the ϵ -Fe₂O₃ phase, two distinct octahedral sublattices are oriented along the a -axis, whereas the third octahedral and the tetrahedral sublattices are oriented antiparallely. Importantly, the magnetization of the tetrahedral sublattice is somewhat lowered (in spite of the same oxidation and spin state of Fe) and the magnetic moments of the sublattices are not fully compensated, leading to the net magnetization of 0.3 μ_B per Fe at 300 K [9]. By preferential substitution of Fe³⁺ at the tetrahedral sites for diamagnetic Me³⁺ cations, it should be possible to increase the magnetization of such particles, improving their performance in various applications, provided that the stability of the phase is not impaired by the dopant, since the relevant properties typically scale with the magnetization. For example, the transverse relaxivity, which represents a basic measure of the contrast effect in T_2 -weighted MR images, is proportional to the magnetization in the limit of the static dephasing regime (SDR) or to the square of the magnetization in the motional averaging regime (MAR) (see, e.g. [10]).

Among the cations with tetrahedral preference, Ga³⁺ poses an attractive choice, moreover, the preferential occupation of the tetrahedral sites in the crystal structure of the epsilon polymorph was evidenced by the first study on the Ga-doped ϵ -Fe₂O₃ by Ohkoshi et al., [11]

who proposed the Ga-doped compound as an efficient millimetre-wave absorber for electronic devices or shielding in wire-less communication. By all means, the proposed dopant does not pose any risk for medical applications due to its insignificant toxicity related to the similarity of Ga^{3+} and Fe^{3+} in terms of the ionic radius and coordination chemistry. Actually, the gallium nitrate has been even used for intravenous injections, under the brand name Ganite, to treat secondary hypercalcemia associated with cancer as Ga^{3+} ions inhibit the activity of osteoclasts. Nevertheless, some surface modification of Ga-doped $\epsilon\text{-Fe}_2\text{O}_3$ nanoparticles is necessary to provide the particles with colloidal stability in aqueous suspensions under physiological conditions. In the plethora of various coating strategies used to prepare colloiddally stable particles applicable in biological systems, possibly even biocompatible in the sense of certain administration modes, the encapsulation of particles into amorphous silica is a basic choice but an outstanding one with respect to model studies. The silica shell is chemically stable, biologically inert, and moreover, it is a very well-defined and simple system compared to complex coatings with complicated polymers or biomolecules. This choice will definitely facilitate the fundamental studies focused, e.g. on the interaction of nanoparticles with cells.

The present study is mainly devoted to the analysis of biological effects of the final silica-coated $\epsilon\text{-Fe}_{2-x}\text{Ga}_x\text{O}_3$ nanoparticles on cell models *in vitro*. The effects of silica-coated nanoparticles on cells have been demonstrated repeatedly in various cancer cell lines of different tissue origin, immortalized cell lines, human and mouse fibroblasts and human peripheral blood lymphocytes [12, 13, 14, 15, 16]. In spite of these numerous reports, only a very limited number of *in vitro* studies have examined the effect of silica-coated particles on

the cytoskeletal structures and their cellular functions [16]. However, the previous studies have reported that various nanoparticles, including titania nanoparticles [17], citric acid and dextran/carboxy dextran-coated iron oxide nanoparticles [18, 19, 20], magnetoliposomes and citrate-coated very small iron oxide particles [19, 20] can affect actin and microtubule cytoskeleton as well as focal adhesion proteins and subsequently the adhesion to the extracellular matrix.

In this work, we investigated the effects of ϵ -Fe_{1.76}Ga_{0.24}O₃ nanoparticles coated with amorphous silica of different thicknesses on cell viability, proliferation, cell cycle distribution, orientation of actin cytoskeleton and formation and maturation of focal adhesions. Naturally, the studied mechanisms of interaction of these nanoparticles with cells have considerable implications for their safe use in biomedical applications.

2 MATERIALS AND METHODS

2.1 Preparation of samples

2.1.1 Synthesis of Ga-substituted ϵ -Fe₂O₃ nanoparticles

Nanoparticles of Ga-substituted ϵ -Fe₂O₃ were achieved similarly as the recently reported undoped sample,[5] i.e. by the preparation of mesoporous silica SBA-15 according to [21], followed by its impregnation with a solution of metal nitrates as in [22], subsequent thermal treatment at a temperature of the epsilon polymorph formation, and, finally, by the removal of the mesoporous template via alkaline leaching. The detailed procedure was as follows. At first, 12 g of P123 triblock copolymer (average $M_r \sim 5,800$, Sigma Aldrich) was dissolved in 450 mL of 1.8 M HCl at 40 °C. After a day of stirring, 25.5 g of tetraethoxysilane (TEOS)

was added dropwise during one hour. The following day, the temperature was raised to 75 °C, and the reaction mixture was agitated and heated further for three days. The material was filtered and thoroughly washed with water. The white solid was dried for two days at 60 °C and calcined at 500 °C for 10 hours. For the impregnation of the so obtained template, 2.04 M solution of $\text{Me}(\text{NO}_3)_3$, where Me stands for Fe and Ga in the molar ratio of 7:1, was prepared by dissolving respective metal nitrate hydrates in water at 50 °C. The impregnation solution was introduced into a stirred hexane suspension of the template while heating to 50 °C. After a day, the impregnation procedure was terminated by decantation and evaporation of the remaining hexane. The product was dried overnight at 80 °C, and the sample was calcined at 1050 °C for four hours. Finally, the silica template was removed by alkaline leaching in 5 M NaOH solution. The particles were separated by centrifugation and were washed at first several times with the 5 M NaOH and then with water acidified to $\text{pH} = 3$ by HNO_3 (1 drop per 1 L of water). The final product was obtained in the form of practically stable suspension of bare particles with the concentration of 18.8 mg/g in the slightly acidified water, further denoted as the parent suspension.

2.1.2 Preparation of silica-coated particles

The encapsulation of Ga-substituted $\epsilon\text{-Fe}_2\text{O}_3$ (ϵFGO) nanoparticles into silica involved their stabilization by citrate and subsequent coating step based on hydrolysis and polycondensation of TEOS. The exact procedure followed the details reported in Ref. [5], four silica-coated products differing in the thickness of the silica shell were prepared by varying the amount of

TEOS employed per the given amount of bare particles. The full procedure is described in the next paragraph.

At first, 50 mg of Ga-substituted ϵ -Fe₂O₃ nanoparticles were separated by exhaustive centrifugation of 2.6 mL of the parent suspension and were dispersed in ice-cold 0.1 M citric acid by application of ultrasound for 15 min. The particles were separated again by centrifugation, were washed with water in one cycle to remove the excessive citric acid, and were redispersed in 10 mL of water alkalized with few drops of ammonia by applying strong ultrasound for 1 h. The suspension of citrate-stabilized particles was transferred dropwise into an ethanol-water-ammonia mixture prepared from 150 mL of azeotropic ethanol, 40 mL of water, and 10 mL of 24 wt% ammonia in a round-bottom flask, which was equipped with a Teflon stirrer and placed in an ultrasound bath tempered to ≈ 46 °C. After several minutes, TEOS was added, specifically 165, 427, 830 and 1650 μ L for the samples ϵ FGO@sil-6, ϵ FGO@sil-11, ϵ FGO@sil-16 and ϵ FGO@sil-24 (the number at the end denotes the mean shell thickness in nm), respectively. The mixture was kept in the tempered bath and stirred mechanically overnight. The raw coated product was separated by centrifugation, and the particles were thoroughly washed at first by ethanol or ethanol-acetone mixtures and then by water in several cycles. Thereafter, the removal of the heavy fraction was carried out by differential centrifugation in three 50 mL tubes at 466 RCF for 15 min. The supernatant was collected as the final product and concentrated to 15 mL, whereas the residue was discarded. According to the chemical analysis of the final aqueous suspensions by inductively coupled plasma mass spectrometry (ICP-MS), the preparatory yield with respect to magnetic cores

was ranging 20–35 wt% (lower for thinner coatings, that were accompanied by slight aggregation, i.e. higher content of the discarded heavy fraction).

2.2 Physical and chemical studies

2.2.1 Fundamental characterizations

The phase composition and the crystal structure of bare particles were analysed by powder X-ray diffraction (XRD). The measurement was carried out on a Bruker D8 Advance diffractometer with Cu K α radiation at room temperature, and the XRD pattern was processed by the Rietveld method in the FullProf program. The accurate chemical composition of the product was determined by X-ray fluorescence (XRF) analysis on an Eagle III μ -Probe spectrometer with Rh-tube.

The size and morphology of particles were studied by transmission electron microscopy (TEM) by using a Philips CM 120 system. Image analysis of micrographs of both bare and silica-coated samples was applied to determine the size distribution of particles. Specifically, the projected areas of particles were accurately measured in the NIS-Elements (Nikon, Tokyo, Japan; employed for bare particles) or ImageJ (employed for silica-coated particles) software, and the corresponding equivalent diameters $d_i = \sqrt{4S_i/\pi}$ were evaluated for: individual particles in the bare sample ($i = cr$), whole silica-coated particles ($i = p$), and magnetic cores of the coated particles ($i = co$). In addition, the distribution of shell thickness (e) was evaluated based on the approximation $e = (d_p - d_{co})/2$ within each coated particle.

The colloidal stability of aqueous suspensions of silica-coated products and their hydrodynamic size were probed by dynamic light scattering (DLS) on a Malvern Zetasizer Nano-ZS instrument. The suspensions were diluted to the same concentration of 0.25 mmol(f.u.) L⁻¹, where f.u. denotes the formula unit of Fe_{1.76}Ga_{0.24}O₃, and were measured at 25 °C three times. The reported values are the means, and the distribution data are based on the measurement with the median Z-average.

Magnetic behaviour of both bare and silica-coated samples was studied in DC fields by means of Quantum Design 14 T PPMS and Quantum Design MPMS XL 7T SQUID systems. For bare particles, hysteresis loops at 5 K and 300 K were measured and temperature dependence of magnetization in the magnetic field of 0.1 T was recorded during cooling from 370 K to 5 K. For the coated products, only the low-temperature hysteresis loops were measured.

The chemical analysis of aqueous suspensions of silica-coated particles was based on the determination of iron by ICP-MS on an Elan DRC-e system (Perkin Elmer). For the decomposition of samples, 1 mL aliquots, weighed on an analytical balance for higher precision, were transferred by concentrated HNO₃ into Teflon vessels, and a mixture of 3 mL of HNO₃ and 1 mL of HF (both Suprapur, Merck, Germany) was added. Microwave decomposition was carried out in a Uniclever BMI-Z device (Plasmatronics, Poland). The decomposed samples were transferred into 50 mL volumetric flasks and after appropriate dilution were spiked with an internal standard solution of ¹⁰⁰Rh. The calibration and the internal standard solutions were prepared from stock solutions with a concentration of 1.000±0.002 g L⁻¹ (Merck).

2.2.2 Relaxometry

The suitability of Ga-substituted ϵ -Fe₂O₃ nanoparticles for MRI was studied based on ¹H NMR relaxometry of aqueous suspensions of the silica-coated products in the magnetic field of 0.47 T by employing a Bruker Minispec 20mq relaxometer (20 MHz). The transverse relaxation time, T_2 , of water ¹H in the suspensions of particles at a concentration of 0.33–0.61 mmol(f.u.) L⁻¹ was determined at the temperatures of 20 °C and 37 °C to enable comparison with literature and to provide data relevant for physiological conditions. CPMG sequence [23, 24] was employed with the echo time TE = 2 ms and repetition time TR = 5 s. The temperature of the sample was adjusted by an external water bath, and the actual temperature was measured directly in the sample. Finally, the transverse relaxivity, r_2 , was calculated according to the equation: $1/T_2(CA) = r_2 \cdot c(CA) + 1/T_2(H_2O)$, where $T_2(CA)$ and $T_2(H_2O)$ relate to the suspension/solution of the contrast agent in water and to pure water, respectively, while $c(CA)$ is the molar concentration of the contrast agent.

2.3 Biological studies

2.3.1 Cell cultures

The human lung adenocarcinoma cell line A549 and human breast adenocarcinoma cell line MCF-7 were obtained from the European Collection of Authenticated Cell Cultures (ECACC, UK). A549 cells were cultured in Minimum Essential Medium Eagle with L-glutamine and

sodium bicarbonate (Sigma-Aldrich, USA) in the presence of 10 % (v/v) fetal calf serum, 1 mM pyruvate, 10 mM HEPES, 50 µg/mL penicillin, and 50 µg/mL streptomycin (all supplements from Life Technologies, USA). MCF-7 cells were maintained in Minimum Essential Medium Eagle with L-glutamine and sodium bicarbonate (Sigma-Aldrich, USA) supplemented with 10 % (v/v) fetal calf serum, 1 µg/mL insulin, 50 µg/mL penicillin, and 50 µg/mL streptomycin (all supplements from Life Technologies, USA). All cell lines were maintained and grown at 37 °C, 95 % humidity, 5 % CO₂. A549 and MCF-7 cells in the maximum range of 20 passages and in an exponential growth phase were used for this study.

2.3.2 Real-time cell proliferation and adhesion assays with the xCELLigence system

The RTCA SP xCELLigence system (Roche and ACEA Biosciences) was used to monitor cell adhesion, proliferation, and cytotoxicity of A549 and MCF-7 cells treated with εFGO@sil-6, εFGO@sil-11, εFGO@sil-16 and εFGO@sil-24 nanoparticles. The system had been tested by a Resistor Plate before the RTCA Single Plate station was placed inside the incubator at 37 °C with 5 % CO₂. First, the optimal seeding concentration for experiments of the A549 and MCF-7 cells was determined. Background measurements were taken by adding 100 µL of an appropriate medium to the wells of an E-Plate 96. Cell suspension (90 µL) was added to each well of the E-plate 96 at the cell density of 4 000 (A549) and 8 000 (MCF-7) cells per well. The cells were monitored every 30 minutes by the xCELLigence system. Approximately 24 h later, when the cells were in the log growth phase, the cells were exposed in triplicates to 10 µL of sterile deionized water with εFGO@sil-6, εFGO@sil-11, εFGO@sil-16 and εFGO@sil-24 nanoparticles to obtain final concentrations of 0.15, 0.31 and

0.61 mmol(f.u.) L⁻¹. Negative controls received sterile deionized water for cell cultures (Lonza), whereas cells treated with 5 % DMSO were used as positive controls. The dynamic cell adhesion, proliferation, and cytotoxicity of the A549 and MCF-7 cells was monitored for a period of 72 h. Data analysis was performed by using xCELLigence 1.2.1 software (Roche and ACEA Biosciences).

2.3.3 Proliferation and viability

A549 cells were seeded at a concentration 5×10^4 cells/1 mL and treated with 0.15, 0.31, 0.61 mmol(f.u.) L⁻¹ of ϵ FGO@sil-6, ϵ FGO@sil-11, ϵ FGO@sil-16 and ϵ FGO@sil-24. Cells treated with topoisomerase II inhibitor doxorubicin (1 μ M) and actin polymerization disruptor cytochalasin D (0.5, 1, 2 or 4 μ g/mL) were used as a positive control. Cell proliferation and viability of A549 cells were determined 48 hours following treatment. The cells were detached with 0.05 % trypsin-EDTA (Life Technologies, USA) for 8 minutes. The trypsin-detached cells were pooled with a medium containing floating cells. Cell membrane integrity was determined using the Trypan blue exclusion technique – mixing 50 μ L of 0.4 % Trypan blue (Sigma-Aldrich, USA) and 50 μ L of cell suspension. Cell counts were carried out using a Bürker chamber and light microscope Nikon Eclipse E200 (Nikon, Tokyo, Japan).

2.3.4 Cell cycle distribution and internucleosomal DNA fragmentation analysis

Where the cell cycle distribution analysis is concerned, the cells were washed with ice-cold PBS and fixed with 70 % (v/v) ethanol. In order to detect low- molecular-weight fragments of DNA, the cells were incubated for 5 minutes at room temperature in a buffer (192 mL of 0.2

M Na₂HPO₄ + 8 mL of 0.1 M citric acid, pH 7.8) and then labelled with propidium iodide in Vindelov's solution for 1 h at 37 °C. DNA content was determined using the flow cytometer CyAn (Beckman Coulter, Miami, FL, USA) with an excitation wavelength of 488 nm. The data were analysed using Multicycle AV software (Phoenix Flow Systems, San Diego, CA, USA).

2.3.5 Immunofluorescence staining

For each condition, 150 000 cells were seeded in 2-well chamber slides SPL (SPL Life Sciences, Korea). After seeding (24 h later), spent medium was replaced with fresh medium and the cells were treated with εFGO@sil-6, εFGO@sil-11, εFGO@sil-16 and εFGO@sil-24 nanoparticles at 0.61 mmol(f.u.) L⁻¹. Cells treated with 2 µg/mL of cytochalasin D were used as a positive control. Following 24-h treatment, the cells were fixed with 4 % (v/v) freshly prepared paraformaldehyde for 10 minutes at room temperature, washed with PBS and permeabilized in 0.2 % (v/v) Triton X-100/PBS (Sigma–Aldrich, St. Louis, MO, USA) for 15 minutes at room temperature. Cells were stained (overnight at 4 °C), with the mouse monoclonal primary antibody anti-paxillin (Life Technologies, USA) and then probed with the donkey anti-mouse-TRITC-conjugated antibody (Jackson ImmunoResearch Laboratories, USA). After pre-incubation with 5.5 % (v/v) donkey serum in PBS for 30 minutes at room temperature, the secondary antibody was applied to each slide and incubated for 1 h in the dark. Cells were then washed three times in PBS and incubated in phalloidin Alexa Fluor 488 (Life Technologies, USA) at in 1 % BSA/PBS (1:40 ratio of phalloidin Alexa Fluor 488 stock solution and 1 % BSA/PBS solution) for 45 min at room temperature. The nuclei were

counterstained with 100 μ l of 4',6-diamidino-2-phenylindole (DAPI) at 1 μ g/mL for 20 min. After three washes with PBS, the slides were mounted with an antifading ProLong® Gold mounting medium (Life Technologies, USA). Images of all of the examined slides were obtained by a Nikon epifluorescence microscope system Eclipse 80i; the exposure time and dynamic range of the camera in all of the channels were adjusted to the same values for all of the slides to portray quantitatively comparable images. Images were further processed, merged and analysed using NIS-Elements Advanced Research 4.13 (instrument and software from Nikon, Tokyo, Japan). For analysis of focal adhesion contacts (FAs) areas, images displaying paxillin staining were background-corrected, thresholded, FAs clusters were identified, and the total respective areas per cell were calculated.

2.3.6 Statistical analysis

The descriptive statistics of the results were calculated, and the charts made in either Microsoft Office Excel 2010 (Microsoft, Redmond, WA, USA) or GraphPad Prism 7 biostatistics (GraphPad Software, La Jolla, CA, USA). In this study, all the values were expressed as arithmetic means with the standard deviation (SD) of triplicates, unless otherwise noted. For quantitative data, normality testing was performed to assess whether parametric or nonparametric tests should be used. For experiments with parametric variables, the significant differences between the groups were analysed using the Student's t-test and a P-value < 0.05 was considered significant.

3 RESULTS

3.1 Structure, composition and morphology of the particles

The XRD analysis of bare nanoparticles evidenced that almost single-phase epsilon polymorph with the $Pna2_1$ symmetry was achieved. The weak diffraction at $2\theta = 24.2^\circ$ (see the XRD pattern in Fig. 1) indicated a minor presence of another polymorph, namely the hematite, whose content was determined to 2–4 %. No signs of the gamma polymorph, maghemite, which is a common admixture in the synthesis of $\epsilon\text{-Fe}_2\text{O}_3$, was observed. The cell parameters of the Ga-doped $\epsilon\text{-Fe}_2\text{O}_3$ were refined to $a = 5.0882(2)$ Å, $b = 8.7787(3)$ Å, and $c = 9.4542(3)$ Å, leading to the cell volume per formula unit of $V/Z = 52.788(3)$ Å³, being only slightly smaller than the value of $52.987(7)$ Å³ reported for undoped $\epsilon\text{-Fe}_2\text{O}_3$ nanoparticles of comparable size and prepared by a similar procedure [5]. Such little effect of the doping is given by the small difference in the size of Fe^{3+} and Ga^{3+} ions; the effective ionic radii of tetracoordinated Ga^{3+} is 61 ppm compared to 63 ppm of the high-spin Fe^{3+} in the same coordination [25]. Importantly, the actual ratio of Fe: Ga in the prepared sample was determined by XRF, based on which the chemical formula was refined to $\text{Fe}_{1.76}\text{Ga}_{0.24}\text{O}_3$.

The morphology of both bare and silica-coated particles is illustrated by transmission electron micrographs in Fig. 2, that are supplemented by the results of the size distribution analysis. The bare $\epsilon\text{-Fe}_{1.76}\text{Ga}_{0.24}\text{O}_3$ particles evinced single-crystalline nature, and their equivalent diameter was characterized by the arithmetic mean of $\overline{d_{\text{cr}}} = 11$ nm and the standard deviation of $sd_{\text{cr}} = 5$ nm while their volume-weighted mean diameter was $\overline{d_{\text{cr},V}} = 17$ nm with the standard deviation of $sd_{\text{cr},V} = 5$ nm. Interestingly, the extensive image analysis indicated that

the size of bare particles is described by the Weibull distribution rather than by the lognormal one (see Fig. 2b).

The silica-coated particles were characterized by a continuous and uniform shell with a smooth surface and no obvious imperfections in the coating. In certain cases, several individual $\varepsilon\text{-Fe}_{1.76}\text{Ga}_{0.24}\text{O}_3$ particles, i.e., several crystallites, were observed within the magnetic core of a single coated particle. Based on the image analysis, three size distributions were determined, namely the distributions of the equivalent diameter of magnetic cores (d_c), of the equivalent diameter of whole silica-coated particles (d_p), and of the thickness of silica shell (e). The basic descriptive statistics are summarized in Table 1. The thickness of the silica shell as well as the size of whole coated particles (see \bar{e} and \bar{d}_p) increased with the amount of the silica precursor, TEOS, employed in the coating procedure of a given amount of magnetic cores, while the standard deviation of the overall particle size (see sd_p) was constant, which demonstrates an efficient control of the geometry of resulting particles. However, the mean size of magnetic cores of coated particles ($\bar{d}_c = 22\text{--}34$ nm) was generally higher than the mean size of individual bare particles ($\bar{d}_{cr} = 11$ nm) due to the aforementioned fraction of particles with several crystallites inside their cores. Considering the negative correlation between \bar{d}_c and \bar{e} , the fraction of such particles was somewhat increasing when decreasing the shell thickness, which can be explained based on a higher probability of aggregation of intermediates with very thin coatings during the growth of silica shells.

Three independent DLS measurements of each coated product provided practically identical hydrodynamic sizes with low and consistent polydispersity indices in the range 0.046–0.149

for all the samples. The distributions of the hydrodynamic size are displayed in Fig. 3, and the Z-average values and polydispersity indices are summarized in Table 1. The hydrodynamic size, representing an apparent size of particles determined from their Brownian motion and thus including also the hydration sphere, was much larger than the overall particle size from TEM and systematically increased with the thickness of the silica shell. At the same time, the distribution became narrower with an increase in shell thickness.

3.2 Magnetic properties and relaxometry

The hysteresis loops of bare ϵ -Fe_{1.76}Ga_{0.24}O₃ particles measured at low and room temperatures are depicted in Fig. 4 together with the loops of undoped ϵ -Fe₂O₃ nanoparticles from Ref. [6] with the mean size $\overline{d_{cr}} \approx 22$ nm and $sd_{cr} \approx 12$ nm. Considering the magnetization in the field of 5 T, the bare Ga-doped particles exhibited specific magnetization of $M(5\text{ K}) = 33.2\text{ Am}^2\text{ kg}^{-1}$ and $M(300\text{ K}) = 22.4\text{ Am}^2\text{ kg}^{-1}$, which is significantly higher than the values observed for the undoped counterpart, $M(5\text{ K}) = 20.8\text{ Am}^2\text{ kg}^{-1}$ and $M(300\text{ K}) = 18.9\text{ Am}^2\text{ kg}^{-1}$, although the mean size of the undoped particles was even larger.

Interestingly, the monotonous increase of the magnetization with decreasing temperature from 300 K to 5 K, with no anomalies at temperatures <160 K, (see the inset in Fig. 4), points to the suppression of the magnetic transition that occurs in the undoped ϵ -Fe₂O₃ system (see, e.g. [9, 26]). On the other hand, the Ga-doped particles still evinced very large room-temperature coercivity of $\mu_0 H_c = 1.2$ T, which was, however, somewhat lowered compared to 2.1 T of the undoped particles. The large coercivity indicated that the nanoparticles of the ferrimagnetically ordered ϵ -Fe_{1.76}Ga_{0.24}O₃ phase, albeit of the mean size as low as $\overline{d_{cr}} = 11$

nm, were characterized by a blocked state, which evidently persisted up to much higher temperatures according to the temperature-variable measurements.

Finally, the measurements of low-temperature magnetization of the silica-coated products enabled us to estimate the weight content of the magnetic phase in the samples. The specific magnetization of the series of coated samples with increasing shell thickness was determined to $M(5\text{ K}) = 19.8, 11.0, 5.8$ and 2.9 emu/g in the magnetic field of 5 T, which corresponded to the weight content of silica, $w_M(\text{SiO}_2)$, as given in Table 1, being in very good agreement with the expectation based on the amounts of reactants employed.

The results of the relaxometric study of aqueous suspensions of the four silica-coated products in the applied field of 0.47 T are presented in Fig. 5. At a given temperature, the transverse relaxivity r_2 decreased with the growing shell thickness, e.g. at the temperature of 20 °C from the value $r_2 = 168\text{ s}^{-1}\text{ mmol(f.u.)}^{-1}\text{ L}$ observed for the $\epsilon\text{FGO@sil-6}$ sample to $r_2 = 89\text{ s}^{-1}\text{ mmol(f.u.)}^{-1}\text{ L}$ for the $\epsilon\text{FGO@sil-24}$ sample. Complementary data at body temperature show also some decrease of r_2 with increasing temperature and repeat the dependence on the shell thickness.

3.3 Biological studies of the effect of silica-coated $\epsilon\text{-Fe}_{1.76}\text{Ga}_{0.24}\text{O}_3$ nanoparticles

3.3.1 Proliferation and viability of A549 and MCF-7 cells

First, cell viability and proliferation were assessed in real time using the label-free xCELLigence system dedicated to adherent cell lines. The xCELLigence system measures cell adhesion, the morphology, viability and number of cells based on impedance, which is

Accepted Article

displayed as normalized cell index (CI) values. Our determinations using xCELLigence assay showed no significant changes in cell index between the negative control and A549 (Fig. 6) or MCF-7 (Fig. 7) cells treated with 0.15, 0.31 and 0.61 mmol(f.u.) L⁻¹ of εFGO@sil-6 or εFGO@sil-11. In contrast, the application of εFGO@sil-16 at 0.61 mmol(f.u.) L⁻¹ decreased the proliferation of A549 cells compared to control, the decrease was more pronounced in the case of MCF-7 cells. This dose-dependent effect was also evident in the εFGO@sil-24 treatment, which at 0.31 mmol(f.u.) L⁻¹ markedly reduced the proliferation of both cell lines compared to the proliferation of control, whereas at 0.61 mmol(f.u.) L⁻¹ it resulted in nearly complete inhibition of cell proliferation.

As a positive control, we compared the inhibitory effect of silica-coated nanoparticles on CI with cytochalasin D at 0.5, 1, 2 and 4 μg/mL. As shown in Fig. 6 and Fig. 7, cytochalasin D induced a drastic CI decrease compared to control A549 or MCF-7 cells in all applied concentrations.

To further verify the antiproliferative and/or *in vitro* cytotoxic activity of the silica-coated nanoparticles, we performed a Trypan blue dye exclusion test by counting the viable cells that exclude the vital stain in Bürker chamber under an upright light microscope. Anticancer drug doxorubicin (1 μM) and cytochalasin D (0.5, 1, 2 or 4 μg/mL) were used as a positive control. The results of Trypan blue assays showed that the application of the studied silica-coated particles at concentrations ranging from 0.15 to 0.61 mmol(f.u.) L⁻¹ had no significant impact on A549 cell proliferation (Fig. 8A) or viability (Fig. 8B).

Comparing the cytostatic activity of the studied particles with doxorubicin and cytochalasin against A549 cells, both positive control treatments showed much stronger ($P \leq 0.05$) growth-

inhibitory activity in all determined concentrations (Fig. 8A). Doxorubicin applied for 48 h also significantly ($P \leq 0.05$) downregulated viability; however, cytochalasin D-treated cells displayed a much lower decrease in the percentage of viable cells, excepting 2 $\mu\text{g/mL}$ concentration (Fig. 8B).

Even though a similar impact of the nanoparticle treatment was expected as previously observed for CI on the xCELLigence system, no considerable effect of the studied nanoparticles on cell viability and proliferation of the A549 cells was evidenced by the Trypan blue exclusion test. One possible explanation of these controversial results could be the impairment of the impedance of electrical current across the cell surface in xCELLigence measurements related to differences in cellular adhesion.

3.3.2 Cell cycle progression of A549 cells

To explore the possible mechanism of growth retardation induced by studied nanoparticles at the highest concentration 0.61 mmol(f.u.) L^{-1} , which could be concluded from A549 cell kinetic experiments performed by using the xCELLigence system, we examined the cell cycle distribution after 48-h incubation with silica-coated samples using flow cytometry. As a positive control, we compared the inhibitory effect of silica-coated nanoparticles on cell cycle progression with doxorubicin (0.4 μM), and cytochalasin D (1 and 2 $\mu\text{g/mL}$). As shown in Fig. 9A and Fig. 9B, no considerable alterations in cell cycle distribution were detected between the control and A549 cells exposed to $\epsilon\text{FGO@sil-11}$, $\epsilon\text{FGO@sil-16}$ or $\epsilon\text{FGO@sil-24}$ at 0.61 mmol(f.u.) L^{-1} . The nanoparticles $\epsilon\text{FGO@sil-6}$ dosed at 0.61 mmol(f.u.) L^{-1} barely (though statistically significantly) changed the percentage of G1- and S-phase populations of

the cell cycle compared to the untreated control cells. However, only doxorubicin and cytochalasin induced a considerable accumulation of cells with a G2 DNA content and a concomitant decrease in G1- and S-phase cells. Moreover, increasing doses of cytochalasin D in A549 cells showed a dose-dependent cell cycle arrest in G2-phase, reaching the highest value at 2 $\mu\text{g/mL}$.

3.3.3 Actin cytoskeleton and focal adhesions of A549 cells

In order to elucidate if the observed decrease in xCELLigence impedance may correlate with the possible morphological changes of A549 cells in response to the exposure to the silica-coated particles, immunofluorescence staining of cytoskeletal protein F-actin and focal adhesion-associated protein paxillin were performed after 24-h interval following treatment. Epifluorescence microscopy analysis and imaging showed disrupted orientation of the F-actin network and a loss of actin stress fibers in A549 cells as a response to $\epsilon\text{FGO@sil-16}$ and $\epsilon\text{FGO@sil-24}$ nanoparticle treatment at 0.61 mmol(f.u.) L^{-1} . The representative microscopic images of A549 cell adhesion assessed by immunofluorescent staining of FA-targeting paxillin as a marker for focal adhesions, cytoskeletal protein F-actin and cell nuclei are presented in Fig. 10. The results of a follow-up quantitative image analysis confirmed a smaller size of cellular FAs areas with significantly decreased values in the cells treated with $\epsilon\text{FGO@sil-16}$ and $\epsilon\text{FGO@sil-24}$ nanoparticles at 0.61 mmol(f.u.) L^{-1} (Fig. 11). The smaller size of FAs is indicative of a reduced capability of adhesion to the extracellular matrix (ECM).

4 DISCUSSION

Importantly, the nanoparticles of $\epsilon\text{-Fe}_{1.76}\text{Ga}_{0.24}\text{O}_3$ phase with the mean size of 11 nm were prepared with the phase purity higher than 95 % according to XRD although the synthesis of the ϵ -phase as a single-phase product, free of α - and γ -polymorphs, is difficult [27]. The composition of the product was practically identical to the ratio of metals used for impregnation of the mesoporous template, i.e., to the target composition. Moreover, the successful incorporation of Ga^{3+} into the crystal lattice of the ϵ -phase was unambiguously proved by magnetic measurements). The magnetic properties of the Ga-doped particles were significantly altered compared to the undoped $\epsilon\text{-Fe}_2\text{O}_3$ and were consistent with the data on the Ga-doped $\epsilon\text{-Fe}_2\text{O}_3$ by Ohkoshi et al. [11]. First, the low-temperature magnetization of the $\epsilon\text{-Fe}_{1.76}\text{Ga}_{0.24}\text{O}_3$ sample was higher by 60 % than the magnetization of a comparable $\epsilon\text{-Fe}_2\text{O}_3$ sample with even larger crystallites (Fig. 4), which can be attributed only to the partial substitution of Fe^{3+} by diamagnetic Ga^{3+} and its preference for tetrahedral sites. Second, the spin-reorientation transition of $\epsilon\text{-Fe}_2\text{O}_3$ at < 160 K was suppressed (see the inset of Fig. 4) in consequence of the doping with Ga^{3+} .

The TEM analysis of the four silica-coated products evidenced that excellent control of their core-shell structure was achieved, providing well-defined samples for the intended relaxometric and biological studies. Further, the DLS measurements evidenced the colloidal stability of their aqueous suspensions, which can be explained in relation to the Coulombic repulsion among the silica-coated particles, whose silanol groups are partially ionized in water under neutral pH [28, 29].

During the evaluation of MRI properties of the coated products in the applied field of 0.47 T, promising transverse relaxivities were determined, namely 89–168 s⁻¹ mmol(f.u.)⁻¹ L at 20 °C and 63–116 s⁻¹ mmol(f.u.)⁻¹ L at 37 °C, i.e. values comparable with commercial contrast agents based on superparamagnetic iron oxides with $r_2 = 33\text{--}189\text{ s}^{-1}\text{ mmol(Fe)}^{-1}\text{ L}$ in the applied field of 1.5 T [2]. Moreover, significant increase in the transverse relaxivity of silica-coated $\epsilon\text{-Fe}_{1.76}\text{Ga}_{0.24}\text{O}_3$ particles is envisaged in higher magnetic fields (magnetic fields of 1.5–4.7 T are typically applied in clinical scanners), as demonstrated on the field-dependence of r_2 for the undoped particles [5].

Although the decrease of r_2 with the silica shell thickness (see Fig. 5) is expected due to the increasing distance of the closest approach of water molecules to magnetic cores, the experimental dependence is anomalous in the view of theoretical expressions derived for the transverse relaxation rate of ¹H in aqueous suspensions of magnetic nanoparticles (see, e.g., [10] for a concise overview). Specifically, if either the motional averaging regime (MAR) or the static dephasing regime (SDR), whose prevalence depends on a number of parameters (the size of magnetic particles, their magnetization and self-diffusion coefficient of water), are considered, we can - under certain assumptions - deduce the following expressions for the dependences of r_2 on the geometrical parameters of particles in MAR or at the SDR limit: $r_{2,\text{MAR}} \propto d_c^2/(1 + 2e/d_c)^4$ and $r_{2,\text{SDR}} \propto (1 + 2e/d_c)^{-3}$. However, these simple models fail to predict the dependence observed in Fig. 5. The actual dependence is certainly complicated by the size distribution of magnetic cores inside the coated particles, but not even the prediction based on the 10th decile of d_c averaged within the set of the coated samples (39 nm) does explain the large deviation. A possible explanation might consist in the fact that

silica is not an impenetrable and inert barrier with respect to water molecules, that may pass into its porous structure and that exchange H^+ with its silanol groups. These processes might lead to a lower effective thickness of the shell compared to its actual geometrical thickness.

In the biological study, we investigated the effect of silica-coated $\epsilon\text{-Fe}_{1.76}\text{Ga}_{0.24}\text{O}_3$ nanoparticles on the viability, proliferation, cell cycle distribution, adhesion and the actin cytoskeleton of A549 and MCF-7 cells. The effect of the nanoparticles on viability and proliferation was assessed by using the xCELLigence system and the Trypan blue exclusion assay. The xCELLigence system measures cell adhesion, morphology, proliferation and viability based on impedance, which is displayed as normalized cell index values [30, 31]. We observed that the $\epsilon\text{FGO@sil-16}$ and $\epsilon\text{FGO@sil-24}$ nanoparticles inhibited both A549 and MCF-7 impedance-based cell properties at higher concentrations of $0.31 \text{ mmol(f.u.) L}^{-1}$ and $0.61 \text{ mmol(f.u.) L}^{-1}$. Surprisingly, no changes in cell proliferation and viability were found by using the Trypan blue exclusion method. Moreover, when the cell cycle analysis was performed by flow cytometry, no marked difference in the cell cycle distribution between the untreated control and the cells treated for 48 h with $0.61 \text{ mmol(f.u.) L}^{-1}$ of silica-coated particles was observed. The inconsistency between the Trypan blue exclusion method and xCELLigence results might be explained by decreasing cell adhesion to ECM or/and cells shrinking due to cytoskeleton alterations, which are not accompanied by disruption of plasma membrane integrity and thus not evidenced by the Trypan blue method.

To confirm this assumption, we performed immunofluorescence microscopy, which evidenced disrupted orientation of the actin cytoskeletal network and a loss of actin stress fibers, as a response to the $\epsilon\text{FGO@sil-16}$ and $\epsilon\text{FGO@sil-24}$ nanoparticle treatment at 0.61

mmol(f.u.) L⁻¹. These results corresponded with other studies that found significant actin cytoskeleton changes after nanoparticle exposure [17, 18, 19, 20]. The disruption of actin cytoskeletal networks in response to εFGO@sil-16 and εFGO@sil-24 nanoparticles might have been related to the uptake of nanoparticles and their accumulation in cells [19] and was assumed to be associated with changes in the FAs formation and maturation [17, 19]. The FAs play a crucial role in the adherence of cells to the ECM connected to the transmembrane protein integrin at one end and to the actin cytoskeleton at the other [32]. Indeed, we observed a significant decrease in FAs area for εFGO@sil-16 and εFGO@sil-24 treated cells. This can further result in a transiently decreased proliferative capacity [20].

5 CONCLUSIONS

To summarize, the data show that high concentrations of silica-coated ε-Fe_{1.76}Ga_{0.24}O₃ nanoparticles with larger shell thicknesses of 16-24 nm interfere with the actin cytoskeletal networks, inducing morphological changes. The particles also significantly decreased FAs areas, which resulted in impaired cell adhesion. Interestingly, application of the same magnetic particles but with thinner coatings of 6–11 nm remained without any significant response. This difference indicates that the observed effect might be of the mechanical nature rather than the chemical one. More specifically, it is not directly connected to the magnetic material used for the study, but more to the amount of matter applied to cells at a given concentration of ε-Fe_{1.76}Ga_{0.24}O₃, rising rapidly with the thickness of the silica coating. These results provide new insight into understanding the biological activity of silica-coated ε-

Accepted Article

Fe_{1.76}Ga_{0.24}O₃ nanoparticles, which promise their safe and beneficial role in biomedical applications.

CONFLICT OF INTEREST

The authors declare that there are no conflicts of interest.

ACKNOWLEDGMENTS

This study was financially supported by the Grant Project No. 18-13323S of the Czech Science Foundation. Furthermore, the work was supported by the Operational Programme Research, Development and Education financed by European Structural and Investment Funds and the Czech Ministry of Education, Youth and Sports (Project No. SOLID21 - CZ.02.1.01/0.0/0.0/16_019/0000760).

REFERENCES

- [1] Qiao RR, Yang CH, Gao MY. Superparamagnetic iron oxide nanoparticles: from preparations to in vivo MRI applications. *J Mater Chem* 2009;19:6274-6293.
- [2] Laurent S, Forge D, Port M, Roch A, Robic C, Vander Elst L, Muller RN. Magnetic Iron Oxide Nanoparticles: Synthesis, Stabilization, Vectorization, Physicochemical Characterizations, and Biological Applications. *Chem Rev* 2008;108:2064-2110.
- [3] Na HB, Song IC, Hyeon T. Inorganic Nanoparticles for MRI Contrast Agents. *Adv Mater* 2009; 21:2133-2148.

- [4] Veverka P, Kaman O, Kacenska M, Herynek V, Veverka M, Santava E, Lukes I, Jirak Z. Magnetic $\text{La}_{1-x}\text{Sr}_x\text{MnO}_3$ nanoparticles as contrast agents for MRI: the parameters affecting H-1 transverse relaxation. *J Nanopart Res* 2015;17:33.
- [5] Kubickova L, Brazda P, Veverka M, Kaman O, Herynek V, Vosmanska M, Dvorak P, Bernasek K, Kohout J. Nanomagnets for ultra-high field MRI: Magnetic properties and transverse relaxivity of silica-coated epsilon- Fe_2O_3 . *J Magn Magn Mater* 2019;480:154-163.
- [6] Jin J, Ohkoshi S, Hashimoto K. Giant coercive field of nanometer-sized iron oxide. *Adv Mater* 2004;16:48-51.
- [7] Machala L, Tucek J, Zboril R. Polymorphous Transformations of Nanometric Iron(III) Oxide: A Review. *Chem Mater* 2011;23:3255-3272.
- [8] Tucek J, Machala L, Ono S, Namai A, Yoshikiyo M, Imoto K, Tokoro H, Ohkoshi S, Zboril R. Zeta- Fe_2O_3 - A new stable polymorph in iron(III) oxide family. *Sci Rep* 2015;5:15091.
- [9] Gich M, Frontera C, Roig A, Taboada E, Molins E, Rechenberg HR, Ardisson JD, Macedo WAA, Ritter C, Hardy V, Sort J, Skumryev V, Nogues J. High- and low-temperature crystal and magnetic structures of epsilon- Fe_2O_3 and their correlation to its magnetic properties. *Chem Mater* 2006;18:3889-3897.
- [10] Carroll MRJ, Woodward RC, House MJ, Teoh WY, Amal R, Hanley TL, St Pierre TG. Experimental validation of proton transverse relaxivity models for superparamagnetic nanoparticle MRI contrast agents. *Nanotechnology* 2010;21:035103.

[11] Ohkoshi S, Kuroki S, Sakurai S, Matsumoto K, Sato K, Sasaki S. A millimeter-wave absorber based on gallium-substituted epsilon-iron oxide nanomagnets, *Angew Chem Int Edit* 2007;46:8392-8395.

[12] Yang W, Lee J, Hong S, Lee J, Lee J, Han DW. Difference between toxicities of iron oxide magnetic nanoparticles with various surface-functional groups against human normal fibroblasts and fibrosarcoma cells. *Materials* 2013;6:4689–4706.

[13] Lankoff A, Arabski M, Wegierek-Ciuk A, Kruszewski M, Lisowska H, Banasik-Nowak A, Rozga-Wijas K, Wojewodzka M, Slomkowski S. Effect of surface modification of silica nanoparticles on toxicity and cellular uptake by human peripheral blood lymphocytes in vitro. *Nanotoxicology* 2013;7:235–250.

[14] Malvindi MA, de Matteis V, Galeone A, Brunetti V, Anyfantis GC, Athanassiou A, Cingolani R, Pompa PP. Toxicity assessment of silica coated iron oxide nanoparticles and biocompatibility improvement by surface engineering. *PLoS ONE* 2014;9:e85835.

[15] Guo X, Mao F, Wang W, Yang Y, Bai Z. Sulfhydryl-modified Fe₃O₄@SiO₂ core/shell nanocomposite: Synthesis and toxicity assessment in vitro. *ACS Appl Mater Interfaces* 2015; 7:14983–14991.

[16] Královec K, Havelek R, Kročová E, Kučirková L, Hauschke M, Bartáček J, Palarčík J, Sedlák M. Silica coated iron oxide nanoparticles-induced cytotoxicity, genotoxicity and its underlying mechanism in human HK-2 renal proximal tubule epithelial cells. *Mutat Res* 2019;844:35-45.

- [17] Ibrahim M, Schoelermann J, Mustafa K, Cimpan MR. TiO₂ nanoparticles disrupt cell adhesion and the architecture of cytoskeletal networks of human osteoblast-like cells in a size dependent manner. *J Biomed Mater Res A* 2018;106:2582–2593.
- [18] Wu X, Tan Y, Mao H, Zhang M. Toxic effects of iron oxide nanoparticles on human umbilical vein endothelial cells. *Int J Nanomedicine* 2010;5:385–399.
- [19] Soenen SJH, Nuytten N, De Meyer SF, De Smedt SC, De Cuyper M. High intracellular iron oxide nanoparticle concentrations affect cellular cytoskeleton and focal adhesion kinase-mediated signaling. *Small* 2010; 6:832-842.
- [20] Soenen SJH, Himmelreich U, Nuytten N, De Cuyper M. Cytotoxic effects of iron oxide nanoparticles and implications for safety in cell labelling. *Biomaterials* 2011;32:195–205.
- [21] Zhao DY, Feng JL, Huo QS, Melosh N, Fredrickson GH, Chmelka BF, Stucky GD. Triblock copolymer syntheses of mesoporous silica with periodic 50 to 300 angstrom pores. *Science* 1998; 279:548-552.
- [22] Imperor-Clerc M, Bazin D, Appay MD, Beaunier P, Davidson A. Crystallization of beta-MnO₂ nanowires in the pores of SBA-15 silicas: In situ investigation using synchrotron radiation. *Chem Mater* 2004;16:1813-1821.
- [23] Carr HY, Purcell EM. Effects of Diffusion on Free Precession in Nuclear Magnetic Resonance Experiments. *Phys Rev* 1954;94:630-638.
- [24] Meiboom S, Gill D. Modified Spin-Echo Method for Measuring Nuclear Relaxation Times. *Rev. Sci. Instr.* 1958; 29:688-691.

[25] Shannon R. Revised effective ionic radii and systematic studies of interatomic distances in halides and chalcogenides. *Acta Cryst A* 1976;32:751-767.

[26] Kohout J, Brázda P, Závěta K, Kubániová D, Kmječ T, Kubičková L, Klementová M, Šantavá E, Lančok A. The magnetic transition in ϵ -Fe₂O₃ nanoparticles: Magnetic properties and hyperfine interactions from Mössbauer spectroscopy. *J Appl Phys* 2015;117:17D505.

[27] Tuček J, Zbořil R, Namai A, Ohkoshi S. ϵ -Fe₂O₃: An Advanced Nanomaterial Exhibiting Giant Coercive Field, Millimeter-Wave Ferromagnetic Resonance, and Magnetoelectric Coupling. *Chem Mater* 2010;22:6483-6505.

[28] Patwardhan SV, Emami FS, Berry RJ, Jones SE, Naik RR, Deschaume O, Heinz H, Perry CC. Chemistry of aqueous silica nanoparticle surfaces and the mechanism of selective peptide adsorption. *J Am Chem Soc* 2012;134:6244–6256.

[29] Kaman, Dědourková T, Koktan J, Kuličková J, Maryško M, Veverka P, Havelek R, Královec K, Turnovcová K, Jendelová P, Schröfel A, Svoboda L. Silica-coated manganite and Mn-based ferrite nanoparticles: a comparative study focused on cytotoxicity. *J Nanopart Res* 2016; 18:100.

[30] Xing Z, Zhu L, Jackson JA, Gabos S, Sun XJ, Wang XB, Xu X. Dynamic monitoring of cytotoxicity on microelectronic sensors, *Chem Res Toxicol* 2005;18:154-161.

[31] Xing JZ, Zhu L, Gabos S, Xie L. Microelectronic cell sensor assay for detection of cytotoxicity and prediction of acute toxicity. *Toxicol In Vitro* 2006;20: 995-1004.

[32] Hall JE, Fu W, Schaller MD. Focal adhesion kinase: exploring Fak structure to gain insight into function. *Int Rev Cell Mol Biol* 2011;288:185–225.

Accepted Article

Captions:

Fig. 1. Powder XRD pattern of bare ϵ -Fe_{1.76}Ga_{0.24}O₃ nanoparticles. The red line shows the calculated pattern based on the Rietveld method, the green line displays the difference between the measured and calculated intensities. Diffractions of the epsilon polymorph (symmetry $Pna2_1$) are indicated by blue vertical lines, whereas the diffractions of the hematite admixture ($R\bar{3}c$) are displayed by red verticals. The inset magnifies the details at lower angles and indicates the position of diffractions of maghemite, whose presence was not supported by the data, by turquoise lines.

Fig. 2. Transmission electron micrographs of bare and silica-coated ϵ -Fe_{1.76}Ga_{0.24}O₃ nanoparticles and their image analysis: (a, b) bare particles, (c, d) ϵ FGO@sil-6, (e, f), ϵ FGO@sil-11, (g, h), ϵ FGO@sil-16, (i, j) and ϵ FGO@sil-24. The size distribution of bare particles is based on the equivalent diameter of individual single-crystalline particles d_{cr} and is fitted by the Weibull and lognormal distribution functions. Each coated product is characterized by size distributions of the equivalent diameter of magnetic cores (possibly containing few crystallites) d_c and of the equivalent diameter of whole silica-coated particles d_p , which are supplemented by lognormal fits, and by the distribution of the thickness of silica shells e with a normal fit.

Fig. 3. The intensity-weighted hydrodynamic size distribution of silica-coated ϵ -Fe_{1.76}Ga_{0.24}O₃ nanoparticles in pure water as determined by DLS measurements.

Fig. 4. Magnetic properties of bare nanoparticles. The hysteresis loops of the ϵ -Fe_{1.76}Ga_{0.24}O₃ sample ($\overline{d}_{\text{cr}} = 11$ nm) at room and low temperatures are supplemented by the loops of similarly prepared ϵ -Fe₂O₃ nanoparticles ($\overline{d}_{\text{cr}} \approx 22$ nm) from Ref. [5]. The inset shows the temperature dependence of magnetization in the field of 0.1 T.

Fig. 5. Transverse relaxivity, r_2 , of aqueous suspensions of silica-coated ϵ -Fe_{1.76}Ga_{0.24}O₃ nanoparticles as a function of the shell thickness, e , in the magnetic field of 0.47 T at the temperatures of 20 °C and 37 °C. The experimental data at room temperature are supplemented by three theoretical predictions of the decrease of r_2 with increasing the shell thickness. MAR and SDR denote the different regimes of transverse relaxation considered, and the parameter d_c gives the size of magnetic cores. (The dotted lines connecting experimental points are just guidelines for eyes.)

Fig. 6. Growth kinetics of human A549 lung carcinoma cells treated with ϵ FGO@sil-6, ϵ FGO@sil-11, ϵ FGO@sil-16, ϵ FGO@sil-24 and cytochalasin D - dynamic real-time monitoring of proliferation and cytotoxicity using the xCELLigence system dedicated to adherent cell lines. The black vertical line indicates the time point when the tested nanoparticles were added. Cells treated with 5 % H₂O were used as vehicle control, whereas

cells treated with 5 % DMSO were used as a positive control. The normalized cell index was measured over 72 h. Plots shown are representative of at least three replicate experiments in each case.

Fig. 7. Growth kinetics of human MCF-7 breast carcinoma cells treated with ϵ FGO@sil-6, ϵ FGO@sil-11, ϵ FGO@sil-16, ϵ FGO@sil-24 and cytochalasin D - dynamic real-time monitoring of proliferation and cytotoxicity using the xCELLigence system dedicated to adherent cell lines. The black vertical line indicates the time point when the tested nanoparticles were added. Cells treated with 5 % H₂O were used as vehicle control and 5 % DMSO treated cells were used as a positive control. The normalized cell index was measured over 72 h. Plots shown are representative of at least three replicate experiments in each case.

Fig. 8. The effect of silica-coated ϵ FGO on the proliferation (A) and viability (B) of human A549 lung carcinoma cells. The changes in the proliferation and viability were determined 48 h after the treatment by using Trypan blue exclusion analysis. Results are shown as the mean \pm SD from three experiments. * - significantly different from the control ($P \leq 0.05$). Cells treated with doxorubicin (1 μ M) and cytochalasin D (0.5, 1, 2 or 4 μ g/mL) were used as a positive control.

Fig. 9. Analysis of the cell cycle after the treatment with silica-coated nanoparticles at mmol(f.u.) L⁻¹. (A) The figure shows representative histograms of human A549 lung

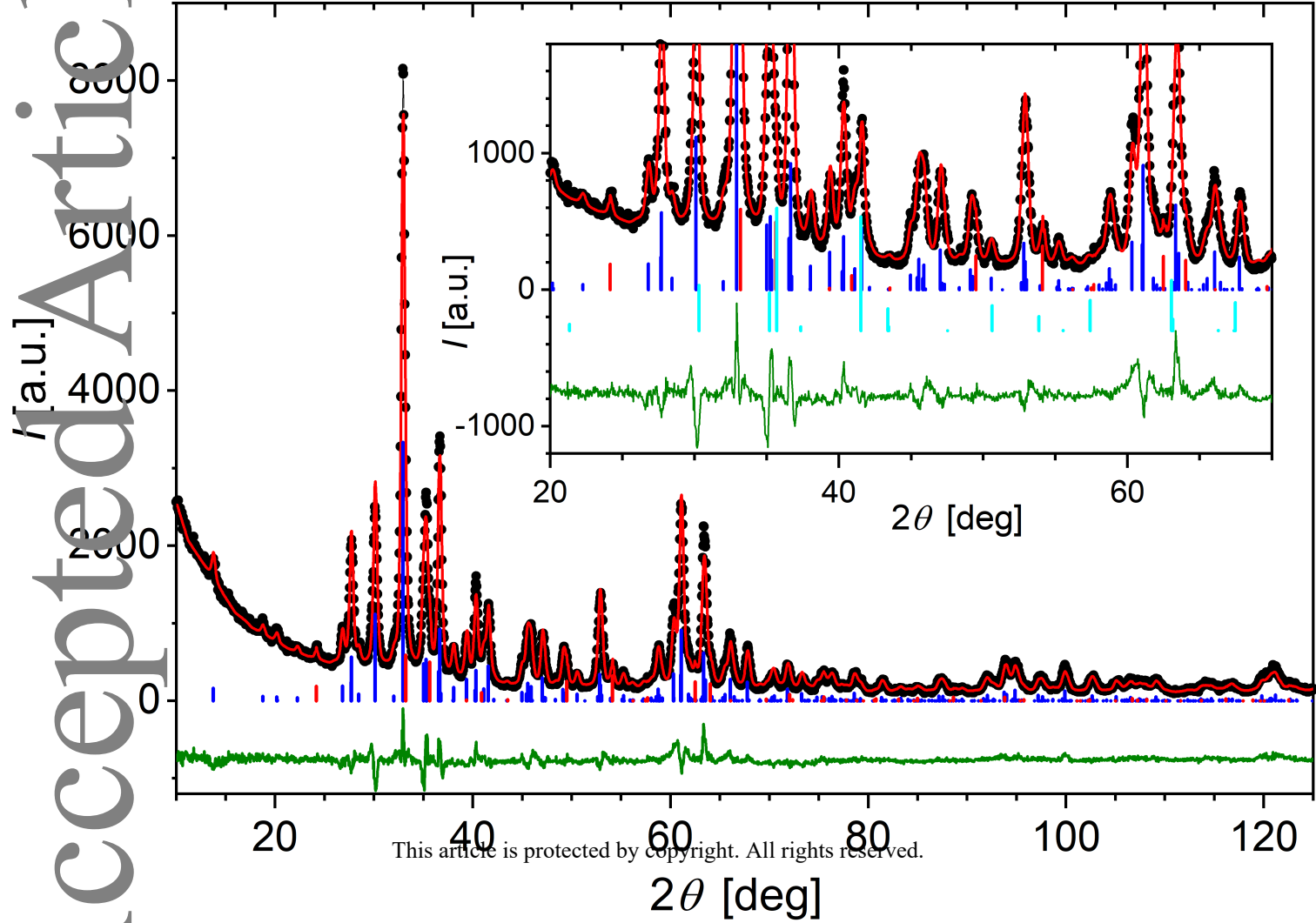
carcinoma cells after the 48-h interval with the mean percentage of cells cycling through phases G1, S, and G2 from flow cytometry measurement of three separate treatments. (B) The bar graph summarizes cumulative data on the percentage of cells in each phase of the cell cycle. Cells treated with doxorubicin (0.4 μ M) or cytochalasin D (1 and 2 μ g/mL) were used as a positive control. Data are presented as mean values \pm SD, n = 3. * - significantly different from the control ($P \leq 0.05$).

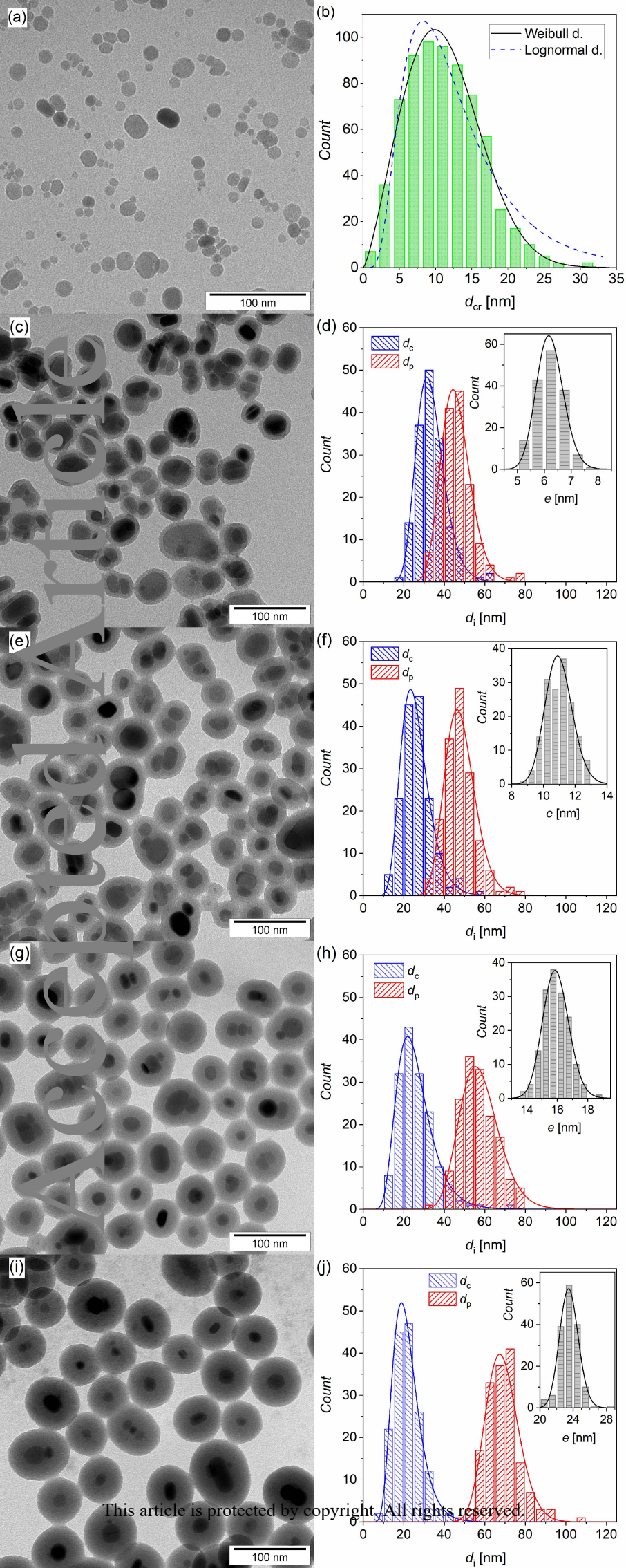
Fig. 10. Fluorescent microscopic images of A549 cells stained with Alexa Fluor 488 phalloidin (F-actin, green), anti-paxillin (red) and counterstained with DAPI (nuclei, blue). The cells were sham-treated with PBS (negative control) or treated with ϵ FGO@sil-6, ϵ FGO@sil-11, ϵ FGO@sil-16 and ϵ FGO@sil-24 at 0.61 mmol(f.u.)⁻¹ L. Cells treated with 2 μ g/mL of cytochalasin D, a member of the cytochalasin fungal alkaloids that acts as a potent inhibitor of actin polymerization, were used as a reference compound in this assay. Experiments were performed in triplicates by using epifluorescence microscopy. Photographs from representative chambers are shown. The scale bar in the images represents 10 μ m.

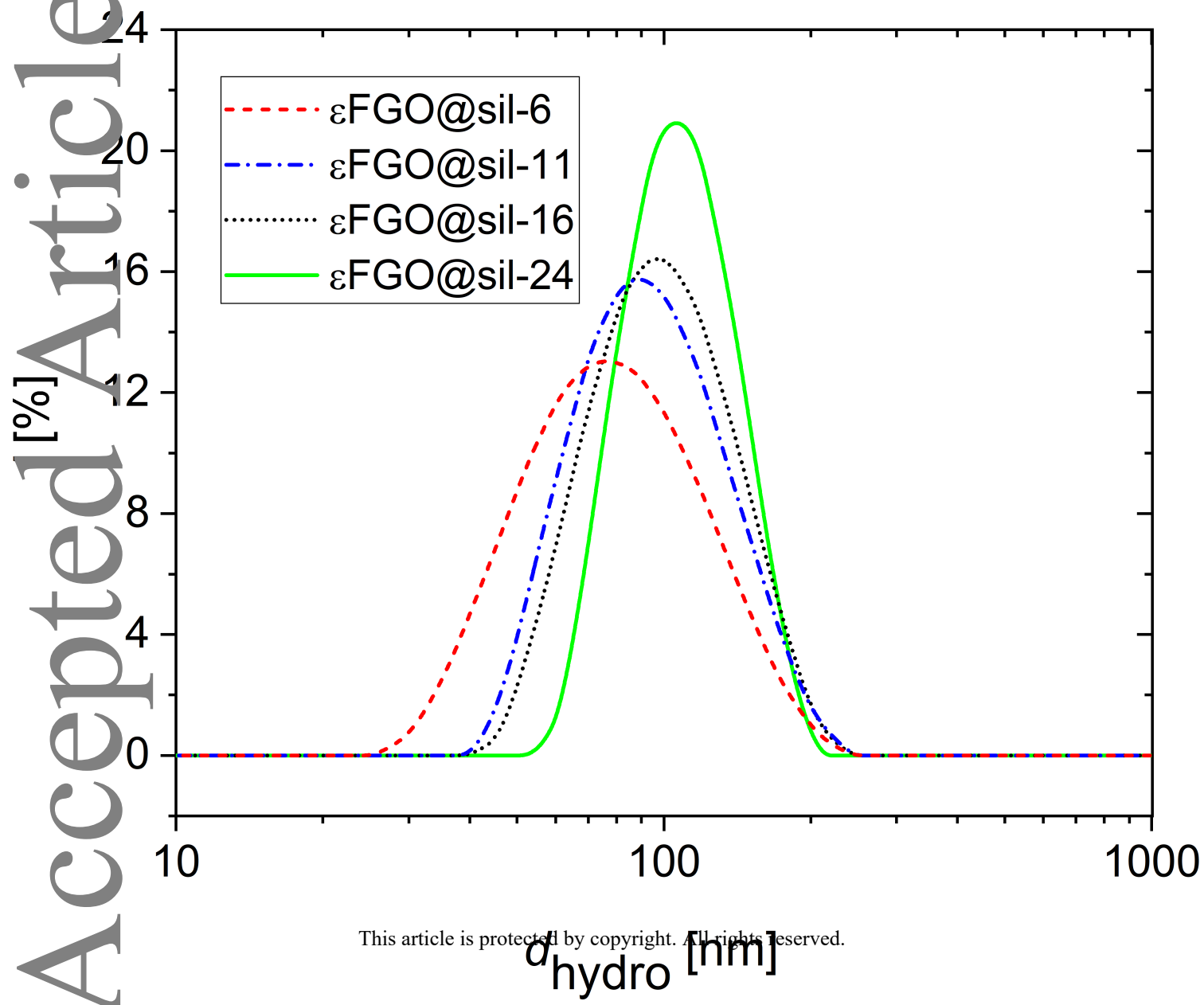
Fig. 11. Histogram representing the cellular FAs areas of control cells or cells treated with the ϵ FGO@sil-6, ϵ FGO@sil-11, ϵ FGO@sil-16 and ϵ FGO@sil-24 particles at 0.61 mmol(f.u.) L⁻¹. Values are represented as the mean \pm SD (n = 10). * significantly different to control ($P \leq 0.05$). Cells treated with cytochalasin D (2 μ g/mL) were used as a positive control.

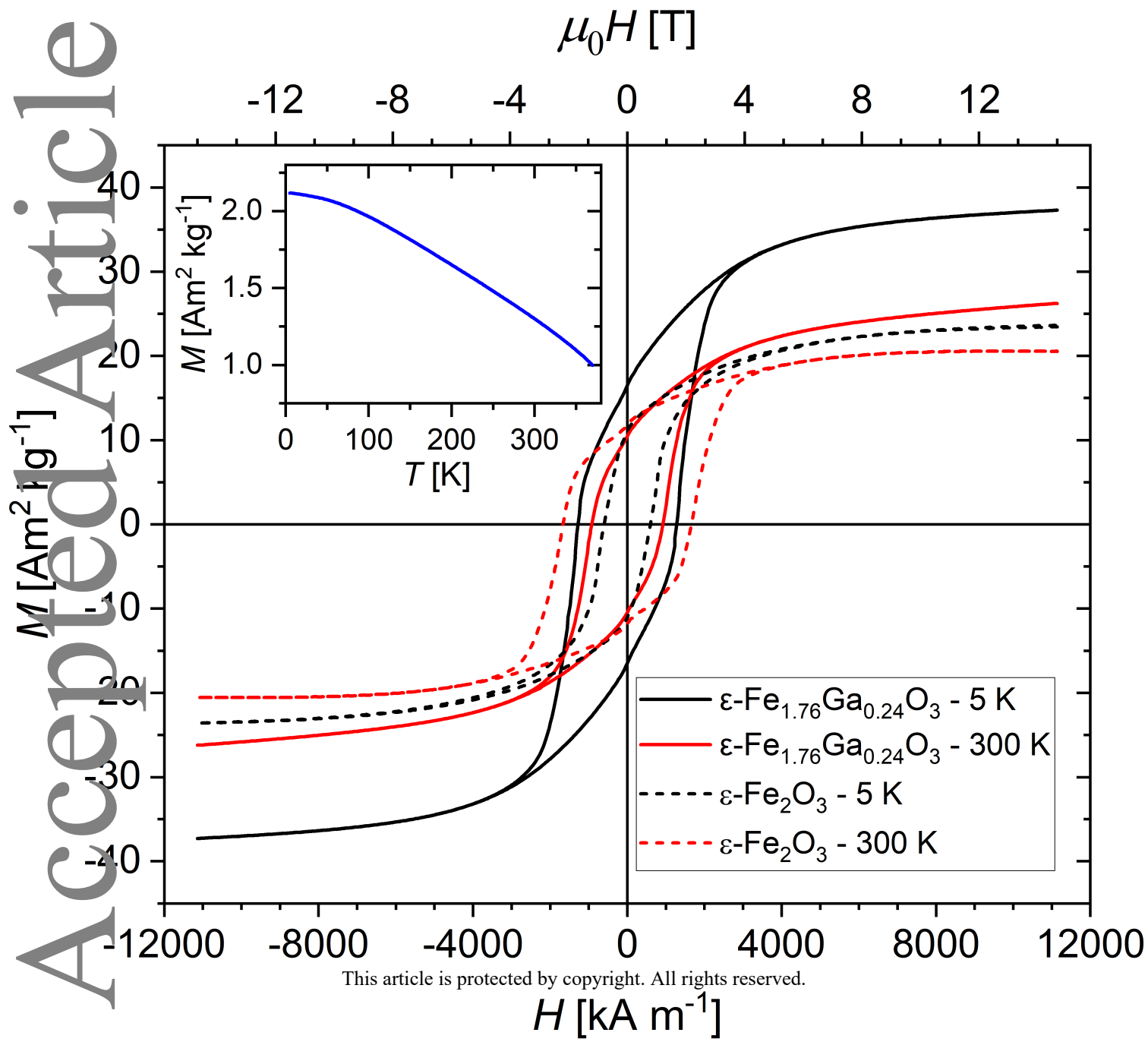
Table 1. Size of silica-coated ϵ -Fe_{1.76}Ga_{0.24}O₃ nanoparticles according to TEM and DLS analyses and expected composition of the particles. The image analysis of the TEM data provided the arithmetic mean of equivalent diameters of magnetic cores and whole silica-coated particles, d_c and d_p , and the mean thickness of silica shell e , with the respective standard deviations denoted as sd_c , sd_p , and sd_e . The theoretical weight content of dry SiO₂, $w_{th}(SiO_2)$, in the products was calculated from the ratio of starting materials employed, whereas the experimental weight of silica, $w_M(SiO_2)$, was obtained from magnetometry at 5 K and 5 T. The hydrodynamic size is described by the Z-average value, d_z , and the polydispersity index, pdi .

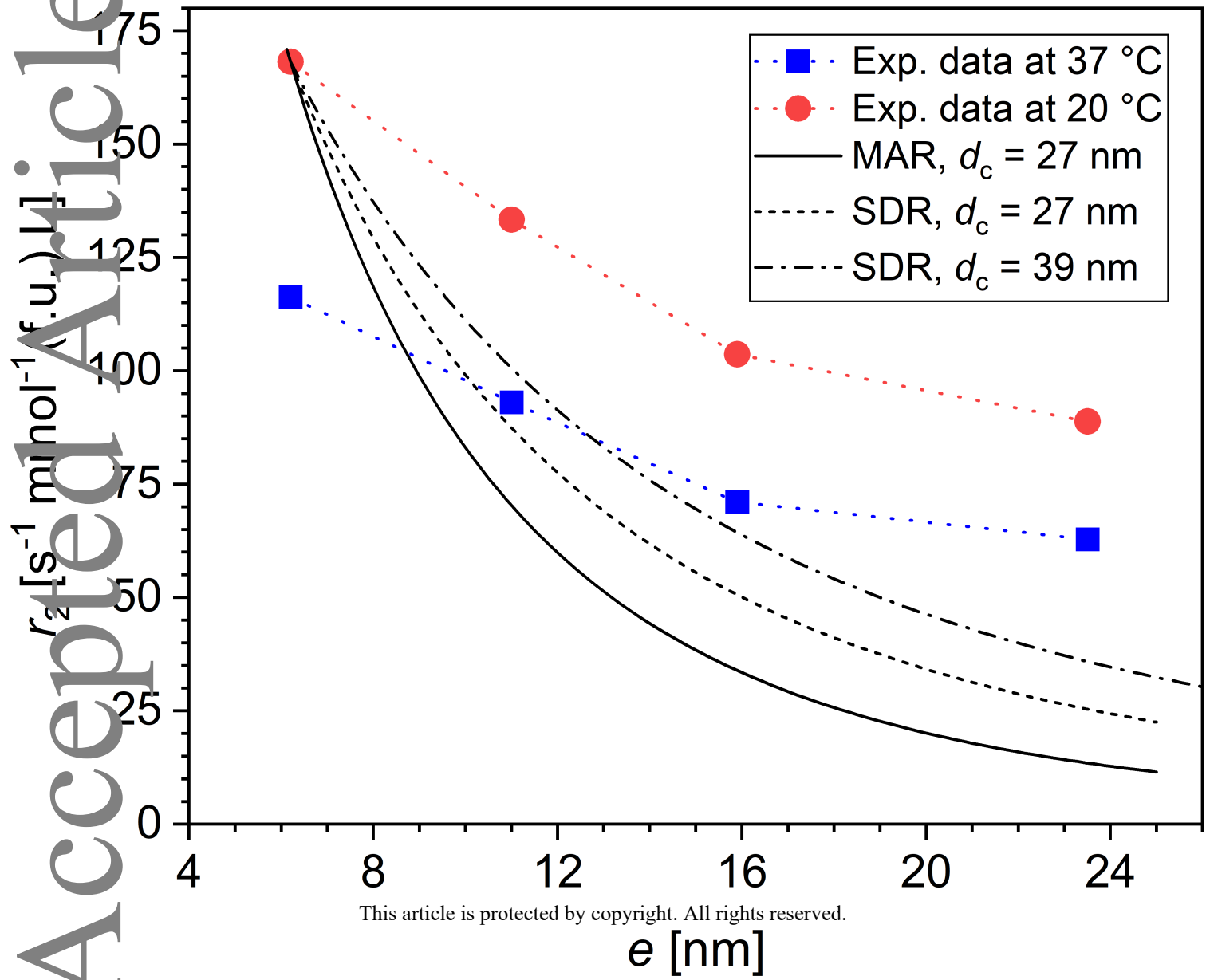
Sample	\bar{d}_c [nm]	sd_c [nm]	\bar{d}_p [nm]	sd_p [nm]	\bar{e} [nm]	sd_e [nm]	$w_{th}(SiO_2)$	$w_M(SiO_2)$	d_z [nm]	pdi
ϵ FGO@sil-6	34	7	46	8	6.2	0.5	0.47	0.40	72	0.149
ϵ FGO@sil-11	26	7	48	8	11.0	0.8	0.70	0.67	88	0.111
ϵ FGO@sil-16	26	9	58	10	15.9	0.9	0.82	0.82	93	0.088
ϵ FGO@sil-24	22	7	69	8	23.5	1.1	0.90	0.91	104	0.046

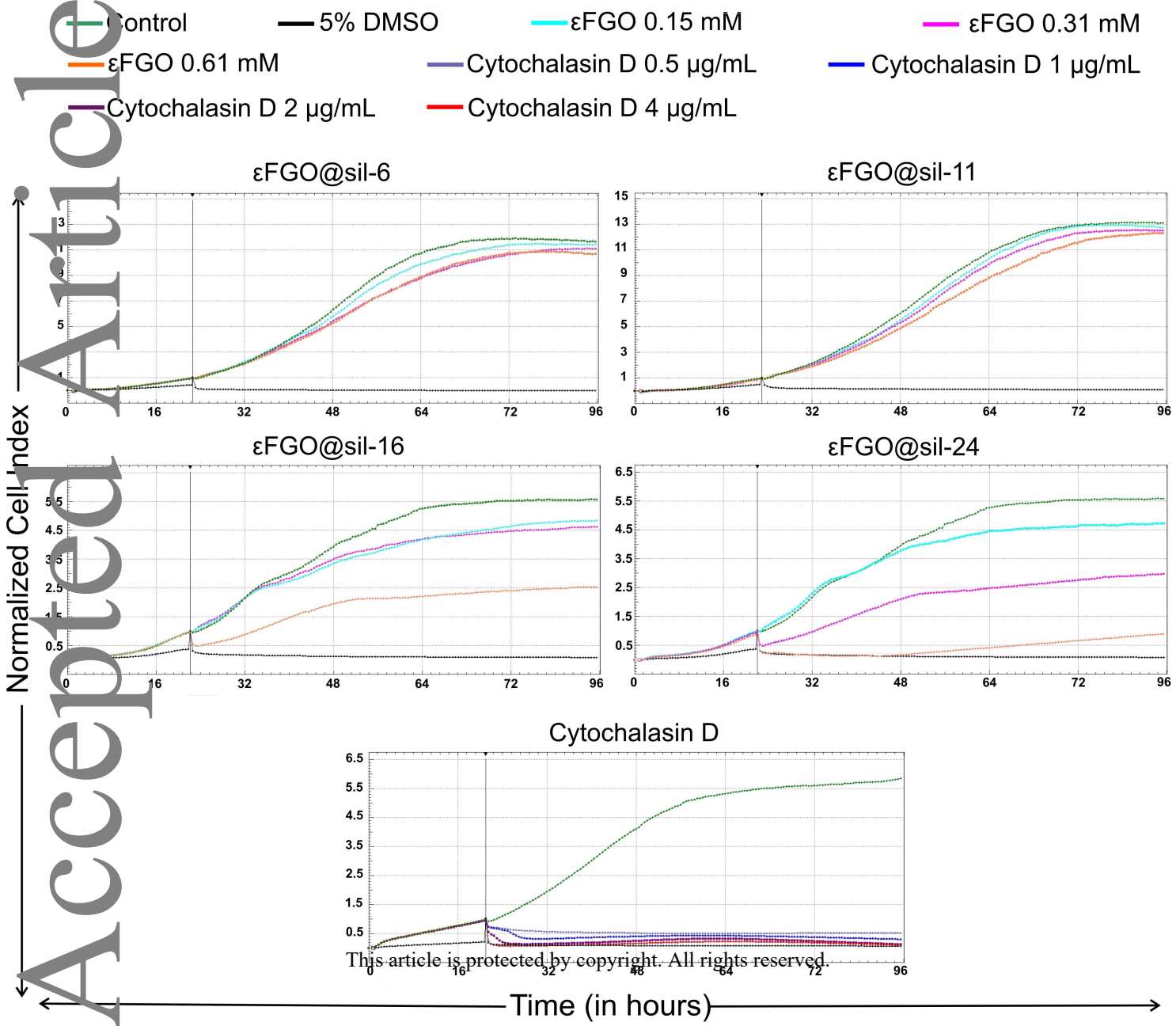


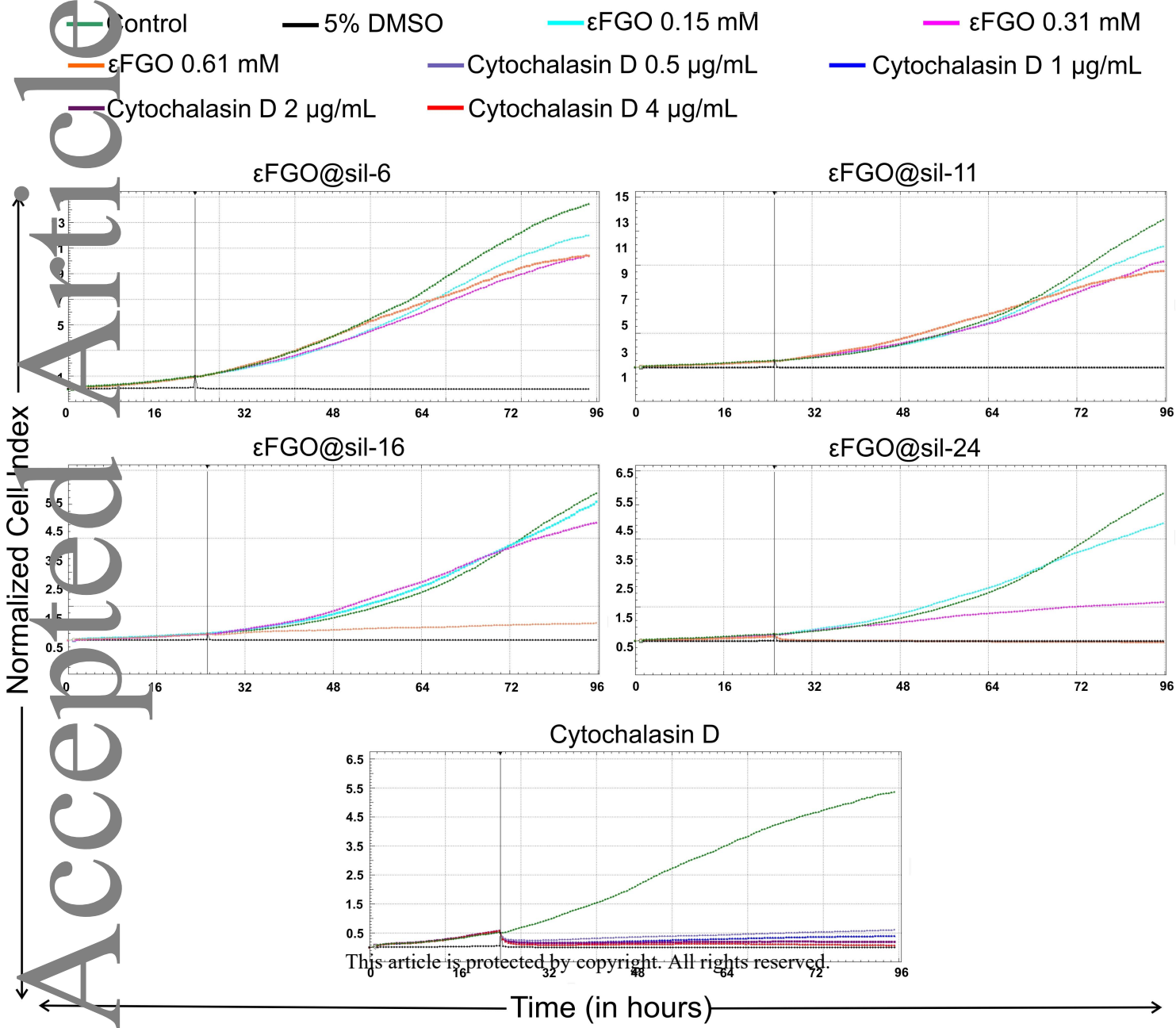








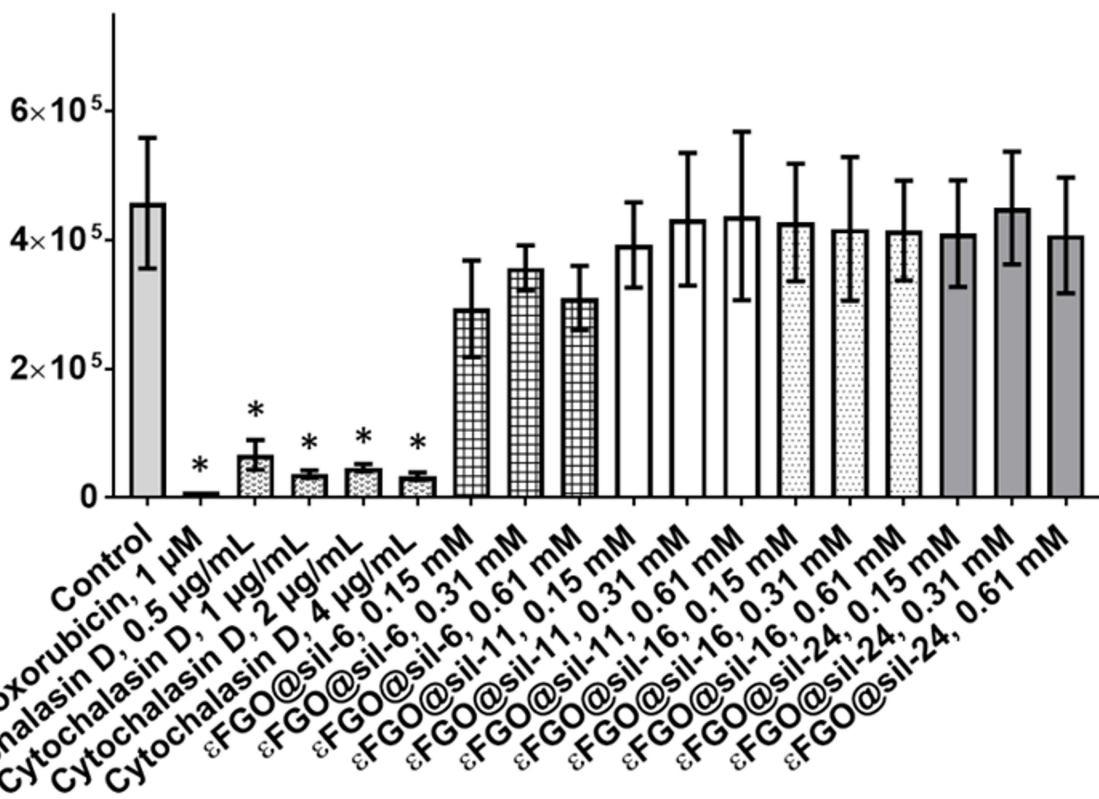




A

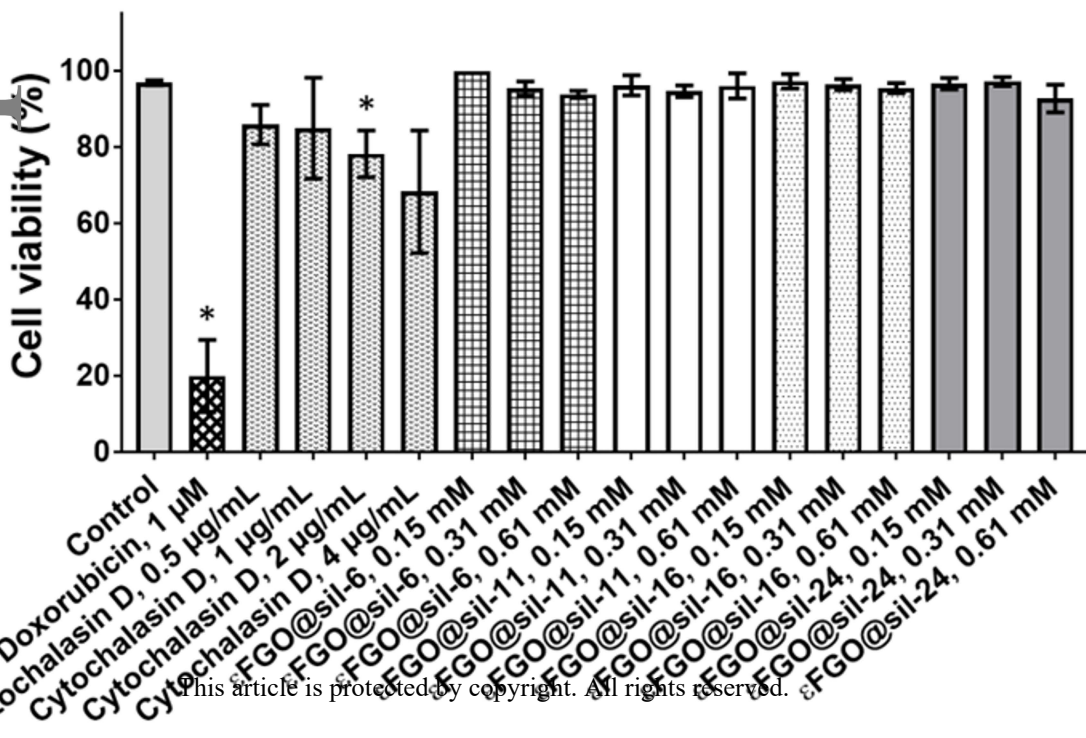
A549

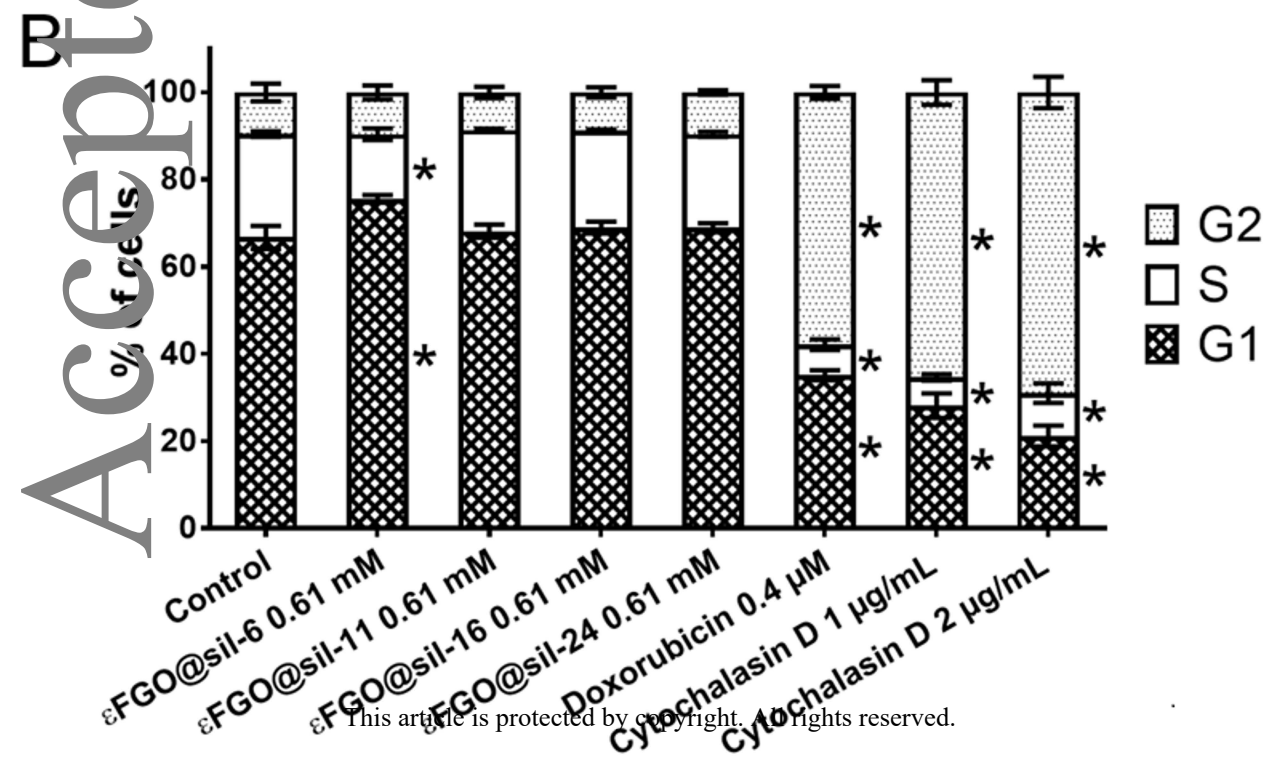
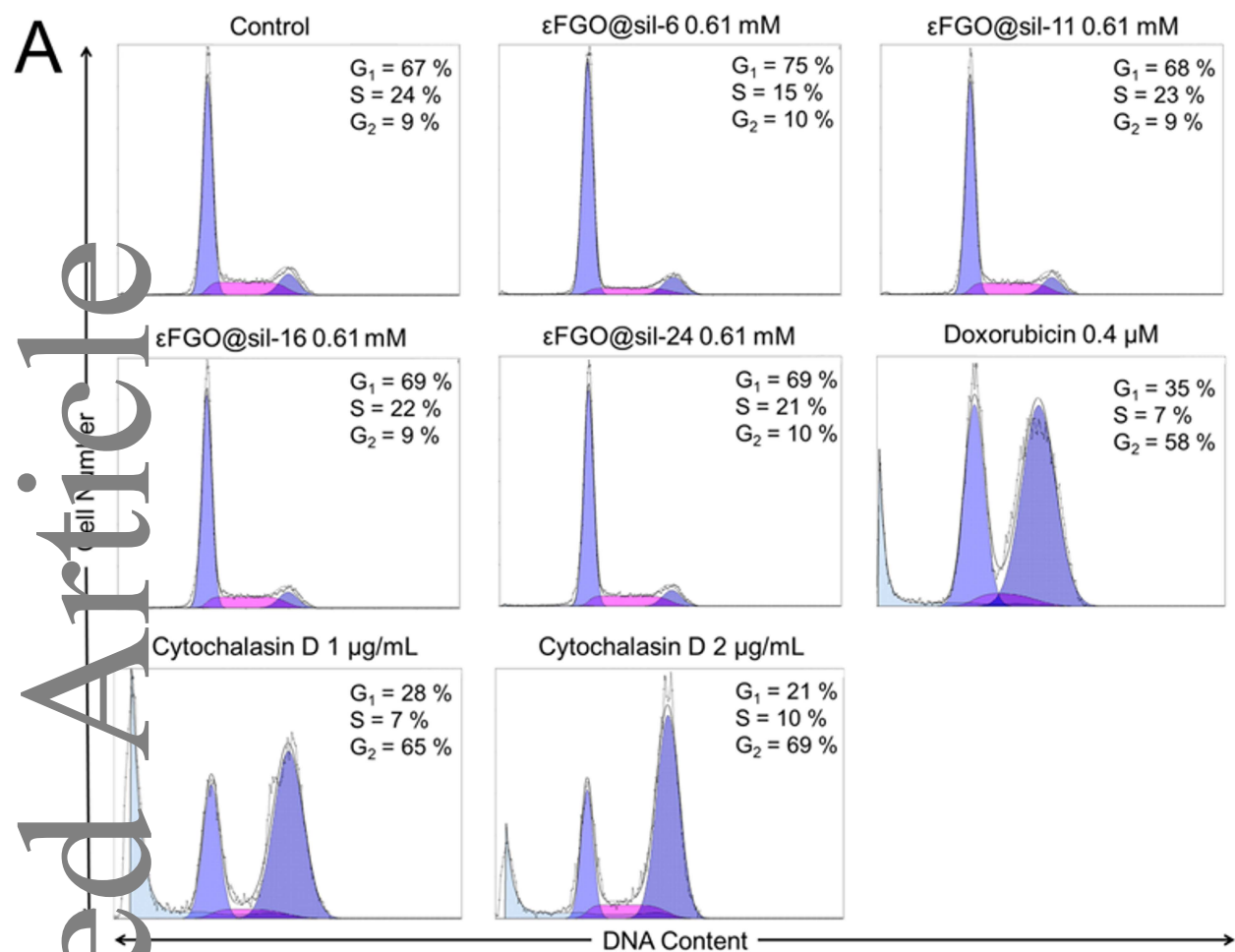
Cell proliferation (number of cells)



B

A549



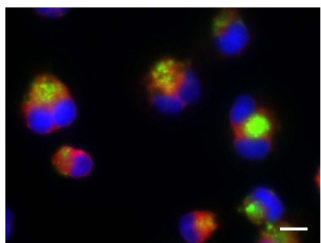
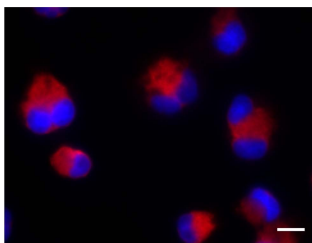
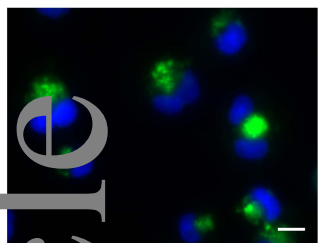


DAPI/Phalloidin

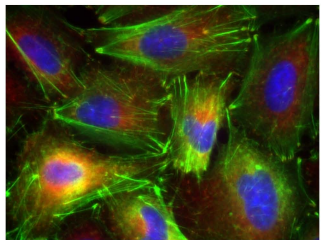
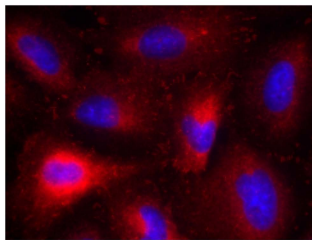
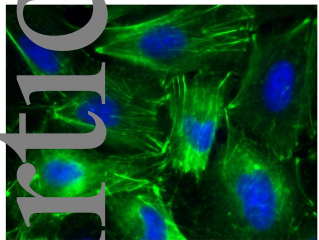
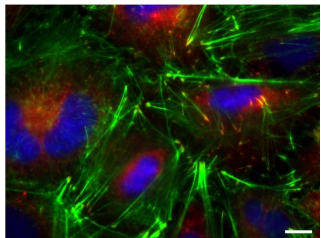
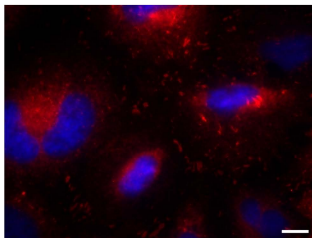
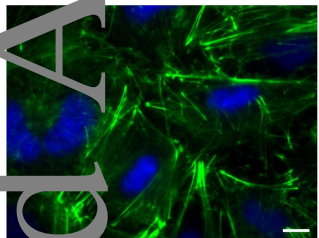
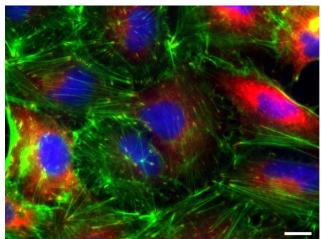
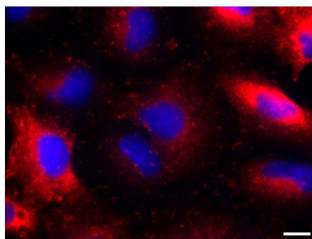
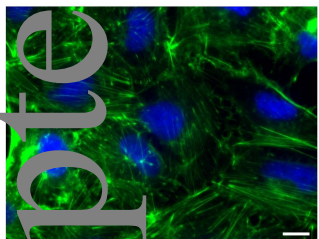
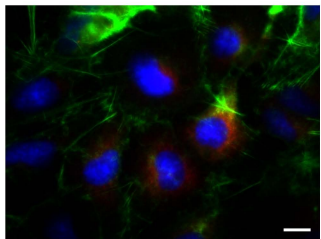
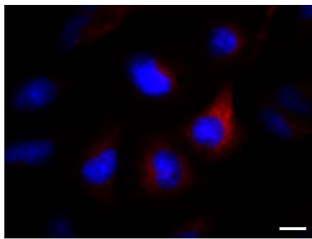
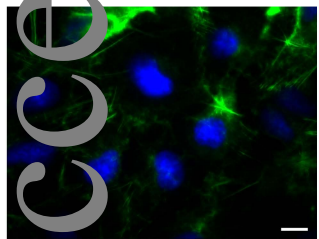
DAPI/Paxillin

DAPI/Phalloidin/Paxillin

Cytchalasin D



Control

 ϵ FGO@sil-6 ϵ FGO@sil-11 ϵ FGO@sil-16 ϵ FGO@sil-24